ARTICLE

Improved Mechanical Stability of Dried Collagen Membrane after Metal Infiltration

Seung-Mo Lee,*,† Eckhard Pippel,† Oussama Moutanabbir,† Ilja Gunkel,†,‡ Thomas Thurn-Albrecht,‡ and Mato Knez*,†

Max-Planck-Institut für Mikrostrukturphysik, Weinberg 2, D-06120 Halle, Germany, and Institut für Physik, Martin-Luther-Universität Halle-Wittenberg, D-06099 Halle, Germany

ABSTRACT A few percent of transition metals impregnated inside some biological organisms in nature remarkably improve such organisms' mechanical stability. Although the lure to emulate them for development of new biomimetic structural materials has been great, the practical advances have been rare because of the lack of proper synthetic approaches. Multiple pulsed vapor phase infiltration proved successful for the preparation of such transition metal impregnated materials with highly improved mechanical stability. The artificially infiltrated metals (Al, Ti, or Zn) from gas phase lead to around 3 times increase of toughness (in terms of breaking energy) of natural collagen in a dried state. In addition, the infiltrated metals apparently induce considerable crystallographic changes in the natural collagen structures. This infiltration approach can be used as guide for the synthesis of bioinspired structural materials related to metal infiltration.

KEYWORDS: multiple pulsed vapor phase infiltration • atomic layer deposition (ALD) • collagen • mechanical stability

INTRODUCTION

Diverse biological organisms, such as insect cuticles and seaworm jaws, have been observed to contain a variety of transition metals like Zn, Mn, Cu, Ca, etc. During the last few decades, the occurrence of such transition metals has been investigated in relation to mechanical properties of those organisms (1, 2). Indeed, the presence and absence of metals appeared to have a critical influence on mechanical properties. Additionally, metal-meditated cross-linking of proteins was proposed to be responsible for drastically enhancing the mechanical properties (3). Although this nature's lesson has deeply inspired material scientists to design new structural materials with great mechanical stability, few practical advances have been yielded because of the extreme difficulties in synthesis. We recently introduced a method to emulate this principle based on multiple pulsed vapor phase infiltration (MPI) which is performed in a conventional system for atomic layer deposition (ALD) (4, 5). By MPI tiny amounts of transition metals were successfully infiltrated into a spider dragline silk, with the resulting silk showing a remarkable improvement of its mechanical properties (4). Here, on the basis of the MPI approach, we infiltrated metals (Al, Zn, and Ti) into dried natural collagen (Figure 1). The resulting metal-infiltrated collagen showed more than 3 times toughness increase as compared to dried native collagen and at the same time showed higher values of ductility (greater than 60% increase) than native collagen in a dried state, resulting in a biopolymer with excellent mechanical stability.

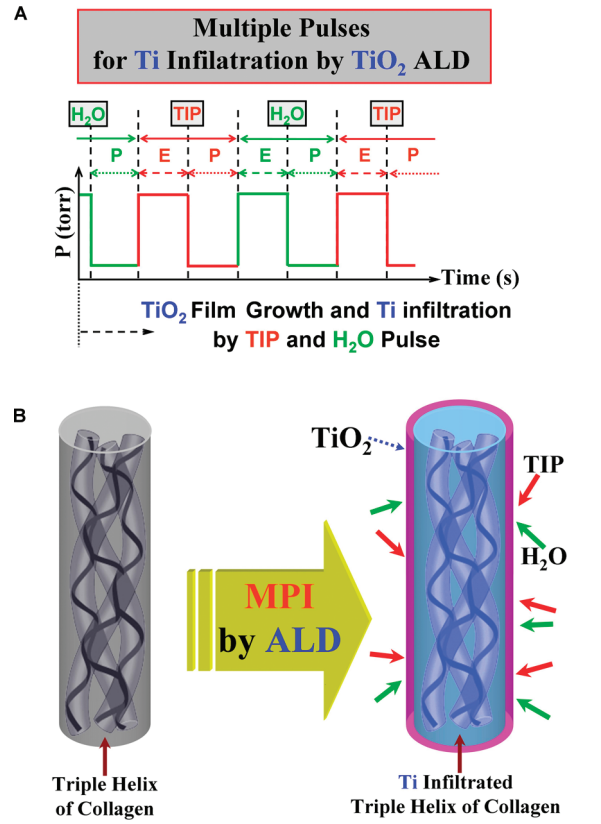

FIGURE 1. Schematic of the multiple pulsed vapor-phase infiltration (MPI) process. (A) Two alternating pulses of reactant vapors, i.e., TIP (titanium isopropoxide, $Ti(OCH(CH_3)_2)_4$) and H_2O (water), are introduced into a vacuum chamber and purged from the chamber in multiple repeating cycles. (B) From the gas phase, Ti can infiltrate soft materials such as collagen tissues and subsequently the physical/chemical characteristics of those materials can be modified. In A, E and P denote exposure and purge, respectively.

* Corresponding author. E-mail: smlee@mpi-halle.mpg.de (S.-M.L.); mknez@mpi-halle.mpg.de (M.K.).
Received for review May 19, 2010 and accepted July 19, 2010
† Max-Planck-Institut für Mikrostrukturphysik.
‡ Martin-Luther-Universität Halle-Wittenberg.
DOI: 10.1021/am100438b

Published on Web 07/30/2010

EXPERIMENTAL SECTION

An overview of the experimental steps is given in Figure S1 and technical details are included in the Supporting Information. The collagen membranes (inner shell membrane) were collected form hen's eggs purchased from a grocery store. The prepared collagen membrane was placed into an ALD reactor (Cambridge Savannah) and dried at 70 °C for 5 min in vacuum (1×10^{-2} Torr) with a steady Ar gas stream (20 sccm). For the infiltration, trimethyaluminum [TMA]($Al(CH_3)_3$)/water, titanium(IV) isopropoxide [TIP] ($Ti(OiPr)_4$)/water, and diethylzinc [DEZ] ($Zn(C_2H_5)_2$)/water (H_2O) pairs were used as sources for the metal and oxygen, respectively. Each cycle was composed of a pulse, exposure and purge sequence for each precursor. For the measurement of engineering stress (σ)−engineering strain (ε) behavior of the prepared samples, all eggshell membrane samples (2 mm × ~20 mm) in a dried state were cut with a knife and mounted in a thick paper jig with a 15 mm diameter hole. A ZWICK 1445 tensile test machine with 500 g HBM load cell was used to measure the ($\sigma-\varepsilon$) curves. The morphology of as-prepared collagen membrane samples was examined by scanning electron microscopy (JEOL JSM-6340F). The characterization of cross sections of the membrane samples (CM/N, CM/Al2O3, CM/ZnO, and CM/TiO2), prepared by focused ion beam (FIB) performed with a JEOL JEM-1010 (100 kV). EDX examinations (line scans and point analyses) were carried out with a Philips CM20FEG and a FEI TITAN 80−300 microscope. Raman measurements of collagen membranes were carried out at room temperature in backscattering geometry with a LabRam HR800 UV spectrometer with following laser lines: 633 nm He−Ne laser, 514 and 488 nm Ar ion laser, and a 325 nm He−Cd laser. For the wide-angle X-ray scattering (WAXS) measurements, collagen membrane samples were attached to a slide glass (76 mm length × 26 mm width × 1 mm thickness) with a soft tape. By means of a conventional laboratory wide-angle X-ray diffractometer (Philips X'Pert MRD with 50 kV, 30 mA) with Ni-filtered CuKα ($\lambda = 1.5421$ Å) radiation, diffraction profiles were measured in 2θ scans. Small angle X-ray scattering (SAXS) experiments were performed using a RIGAKU rotating anode. The X-ray beam was monochromated with an Osmic X-ray optics ($\lambda = 1.5421$ Å). The size of the beam on the sample was approximately 300−500 μm. The samples were placed in a chamber which was evacuated to a pressure of approximately 1×10^{-1} mbar. A SIEMENS area detector of 1024 × 1024 channels was used to count the scattered intensity. Typical measuring times were 90 min. All measurements were performed at room temperature.

RESULTS AND DISCUSSION

Collagen is one of the most abundant proteins on earth, in particular mammals, and can exhibit large varieties in shape and size (6). The distinctive marker of collagen is the composition of three polypeptide chains, each of which contains regions with a repeating amino acid motif [Gly-(Glycine)-X-Z], where X and Z stands for any amino acid. Frequently, X and Z are proline (Pro) and hydroxyproline (Hyp), respectively (7−11). Each polypeptide chain (α-chain) has left-handed helical conformation with three identical α-chains constituting a right-handed coiled-coil triple-helical structure (see Figure S2 in the Supporting Information). Among diverse collagens, the fibrillar collagen (primarily type I collagen) is of most interest for both life science and materials science, because it forms most of the connective tissues in vertebrate body such as skin, tendon, lung, ligament, bone, cornea, and vasculature (6−12).

In this experiment, we chose natural collagen membranes, which were conveniently extracted from ordinary

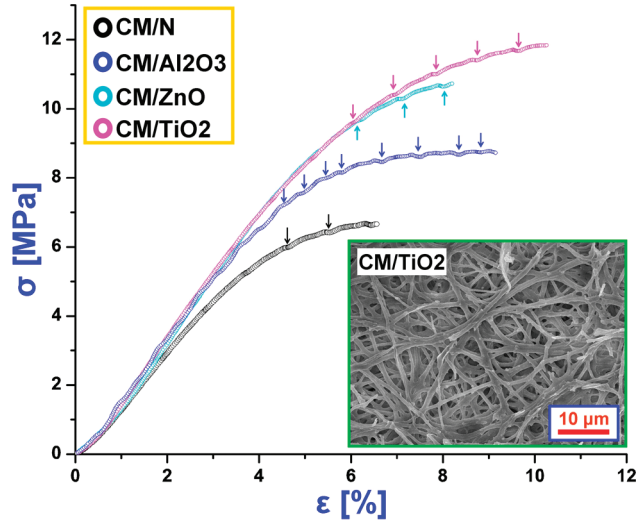

FIGURE 2. Deformation behavior of metal infiltrated (Al, Zn and Ti) collagen membranes under the uniaxial tensile test. Sample denotations and fracture stress/strain, yield stress/strain and toughness values can be found in Tables S1 and S2 in the Supporting Information. The arrows on each stress−strain curve mark sawtooth patterns (see details in the text). Inset: SEM image of a Ti infiltrated (CM/TiO_2) membrane.

hen's eggs (which is primarily composed of type I and V collagen) (13−15). We collected the membrane from the air cell region of the egg having no contact with the calcite shell of the egg (see the Experimental Section). In the ALD reactor, the collected collagen membranes were alternately exposed to multiple pulse pairs, $Al(CH_3)_3/H_2O$, $Ti[OCH(CH_3)_2]_4/H_2O$, and $Zn(C_2H_5)_2/H_2O$, for the infiltration of Al, Ti, and Zn, respectively. Subsequently, by uniaxial tensile tests, the mechanical properties of Al, Ti, or Zn infiltrated collagen membranes were examined (see Figure 2, and for sample denotation and mechanical data, see Tables S1 and S2 in the Supporting Information). Although under uniaxial tension (16), the toughness and fracture strain of CM/N were around 23 MJ/m^3 and 6.1%, respectively, the values for metal infiltrated collagen membranes rose to ranges 52−77 MJ/m^3 and 8.1−10.2%. Among the treated collagen membranes, the Ti infiltrated ones (CM/TiO2) showed the strongest improvements in terms of both toughness and ductility and therefore will be discussed in more detail. Data for collagen membranes infiltrated with Al (see Figure S3 in the Supporting Information) and Zn (Figure S4 in the Supporting Information) can be found in the Supporting Information.

Looking at the stress−strain curves, a noteworthy feature of the infiltrated collagen membranes are sawtooth peaks (marked by arrows in Figure 2), which although the length scale is different are also frequently observed in similar measurements of further biomaterials such as titin (17), spectrin (18), abalone shell (19), and tenascin (20). The number of observable sawtooth peaks increases after the metal infiltration. Presumably, the increase of the number of those peaks induced by the stress fluctuation can be a matter of the rupture of a larger number of metal-mediated interprotein bonds or the slip pulse of interfibrillar cross-links inside the collagen membrane, originating from the metal infiltration. One may also wonder whether the observed

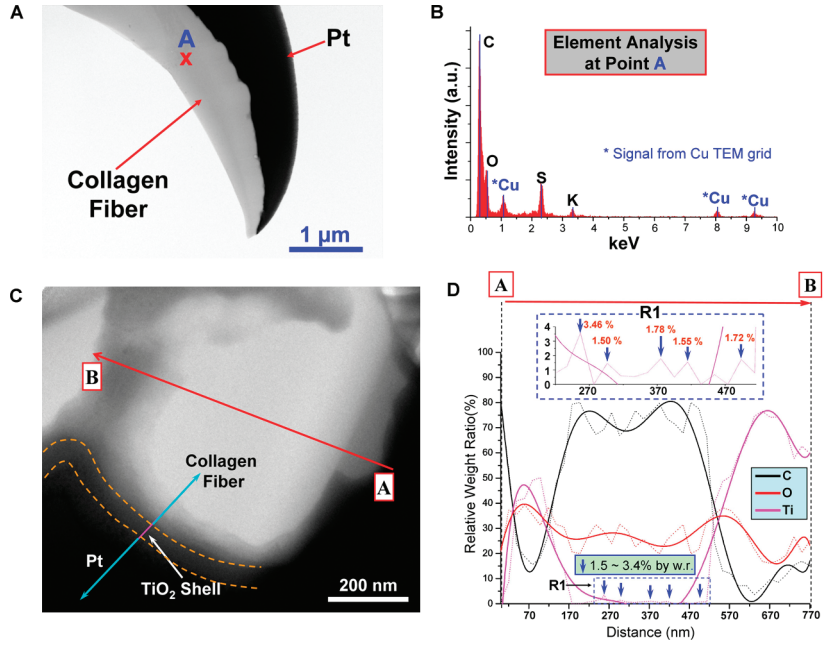

FIGURE 3. Scanning transmission electron microscopy (STEM) images and corresponding energy-dispersive X-ray (EDX) analysis. (A) STEM image of a cross sectioned native collagen fiber of CM/N prepared by focused ion beam (FIB) using platinum (Pt) as an electrode. (B) EDX point analysis spectrum measured at position A in panel A. (C) STEM image of a cross-sectioned Ti infiltrated collagen fiber (CM/TiO2). (D) Element concentration profile from EDX analysis scanned along the line from A to B in image C. The dotted lines are actual data and the corresponding solid line is an interpolated curve using those data.

increase in fracture strength of the infiltrated porous collagen membranes is related to the metal oxides (Al_2O_3, TiO_2, or ZnO) that are covering and interconnecting the collagen fibers. However, this seems to be not the case. It rather appears to be related to the increase in cross-linking densities inside collagen induced by the metal infiltration (the discussion will follow further below).

By STEM-EDX (scanning transmission electron microscopy-energy dispersive X-ray) point analysis of a cross-sectioned (by focused ion beam) native collagen membrane (CM/N), S and K aside from C, O, and H could be identified (Figure 3A, B). In the case of CM/TiO2, as shown in Figure 3C, a gradient in the mass concentration of Ti between the TiO_2 shell layer and the bulk collagen was observed. In some regions, it was difficult to discriminate the boundary between the TiO_2 shell and the collagen. From an EDX line scan from point A to B in Figure 3C, it could be derived that in proximity to the TiO_2 shell layer the collagen contains a substantial amount of Ti. In the central region, a weaker signal (1.5−3.4% by atomic weight ratio), but still above the resolution limit of the EDX (0.5−1.0%), was observed (21). The exact infiltration mechanism during MPI and the potential binding sites for Ti are not yet clear. However, several effects might be considered to be responsible for the significant modification of the bonding structure of the collagen. Those effects include the severe attack of water at elevated temperatures occurring at the hydrogen bonds (22) that interconnect the three polypeptide chains in the triple helix of the collagen. The resulting global weakening of the hydrogen bonds (23), the strong reactivity of titanium isopropoxide (TIP, $Ti[OCH(CH_3)_2]_4$) with amines and hydroxyl groups, and the metal ions' affinity to bind to the proteins (24) are assumed to lead to Ti−collagen interactions (24−28).

In addition, a high level of cysteine with thiol groups was found in the hen's collagen membrane (29). The thiol groups (−SH) tend to be excellent ligands for many metals and are also potential binding sites for Ti or Zn. New bonds are presumably formed by mediation of Ti, which can also be derived from Raman shifts of the Ti infiltrated collagen (see Figure 4 and Figure S5 and Table S3 in the Supporting Information).

Raman spectra of the collagen membranes (Figure 4) show signals from amide I (1668 cm^{-1}) and amide III (1271 cm^{-1}) (30), (C−C) stretching modes of the ring of Hyp and Pro at 875 and 855 cm^{-1} and the vibration mode at 1582 cm^{-1} which can be assigned to Pro and Hyp (31). The data support the presence of a helical conformation in the collagen of the hen's eggshell membrane (30, 32). Interestingly, some changes are detected for Ti-infiltrated collagen membranes. In particular, a decrease of the amide I (C═O stretching) and amide III (N−H bending) band intensities for the Ti infiltrated collagen can be observed (Further changes and the corresponding assignments can be found in Table S3 in the Supporting Information). It is known that although its coiled-coil triple helix structure is dominated by hydrophobic interactions, the responsible interactions for stabilizing collagen are hydrogen bonds. In triple helices, each individual α-chain is stabilized by Pro and Hyp, and the trimerization of α-chains is favored by close packing and intermolecular hydrogen bonding. There is only one hydrogen bond per Gly-X-Z triplet, namely, between the amine group of Gly and the carbonyl group of the residue in position X. The remaining two backbone carbonyl groups in each triplet and any backbone amine group of X and Z are not involved in hydrogen bonding (33). Vapor phase TIP and water might affect the hydrogen bonds connecting Gly and

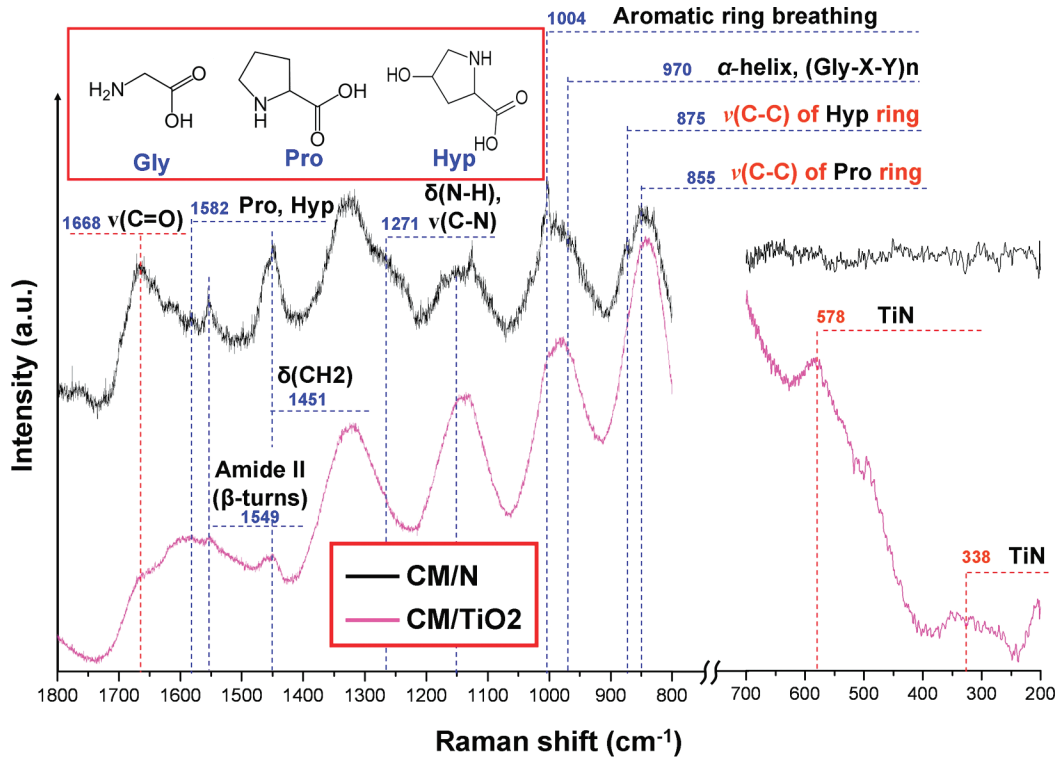

FIGURE 4. Raman spectra of a native collagen membrane and a Ti infiltrated collagen membrane in the region of 1800 to 800 and 700 to 200 cm^{-1}. Raman shifts and corresponding tentative assignments of further samples can be found in Figure S5 and Table S3 in the Supporting Information. Key to Abbreviation: ν(stretching), δ(bending) and π(twisting).

X in a way as the (presumably N−H···O═C) bonds are weakened and hydrogen is substituted with Ti. The newly formed bonds, mediated by Ti, are stronger than hydrogen bonds (see the schematic drawings in Figure S6 in the Supporting Information). This assumption is also supported by Raman spectra particularly from the shifts at 578 and 338 cm^{-1}, which can tentatively be assigned to vibrational modes of a Ti−N bonding (right figure in Figure 4) (34). In addition, X-ray scattering patterns of CM/TiO_2 show crystallographic changes presumably caused by Ti-mediated bonding between nitrogen and carbonyl groups.

In the X-ray scattering patterns of CM/N, protein crystal structures were observed from reflections (peak A of CM/N in Figure 5, see details and further data in Figures S7 and S8 and Table S4 in the Supporting Information). The value of spacing (d) was around 3.0 Å, which may correspond to the translation length per one amino acid in a single α-chain of the collagen (see the schematic drawing in Figure S2 in the Supporting Information) (8−11). Peaks B and C can potentially be associated with the diffraction between the separate chains (35). It can be observed that the crystal structure of the collagen membrane is notably changed after Ti infiltration: two new peaks, D (d = 5.30 Å) and E (d = 6.31 Å), were observed with an intensity of D being stronger than of peak A. This means that the change is quite pronounced. Considering the spacing of 5.30 Å and helix parameters of the collagen models by Rich et al. (8) and Fraser et al. (10), this distance is very close to the vertical distance of hydrogen bonds [$(N-H)_{Gly}\cdots(O{=}C)_{Pro}$] connecting single collagen α-chains (see detailed parameters for the helix in refs 8 and 10 and a schematic drawing of the atomic arrangements in

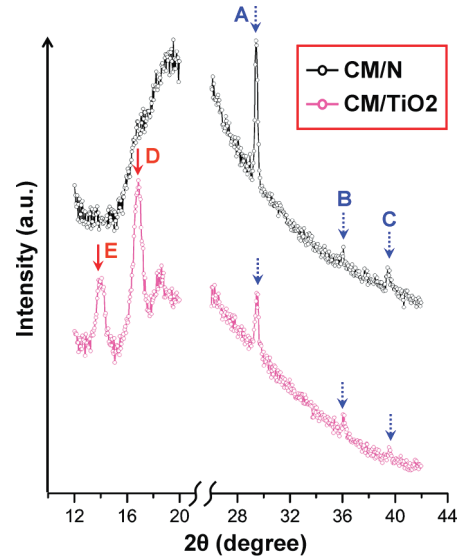

FIGURE 5. Wide-angle X-ray scattering (WAXS) pattern of a native collagen membrane and a Ti infiltrated membrane. WAXS pattern of Al or Zn infiltrated collagen can be found in Figure S7 in the Supporting Information. The detailed data, such as 2θ position and corresponding plane spacing, together with spectra comparison of each membrane are summarized in Table S4 in the Supporting Information. The spectra are vertically shifted for clarity.

Figures S2 and S6 in the Supporting Information). In agreement with the Raman observations, after Ti infiltration the intrahelical hydrogen bonds of collagen are most likely to be broken or transformed into new Ti mediated bonds (N−Ti···O═C), as shown in Figure 6. According to the strong peak intensity, the newly formed bonds should have a very high regularity.

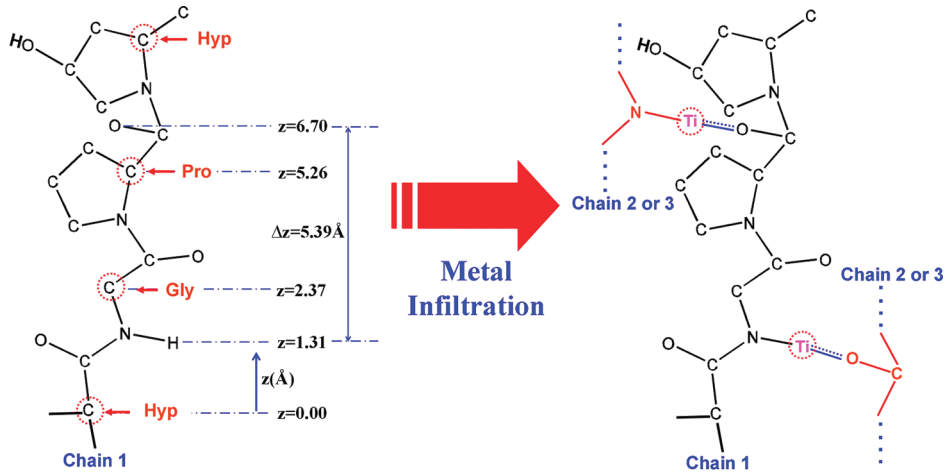

FIGURE 6. Speculative conformational change of collagen molecules after metal infiltration. The repeating sequence is Gly-Pro-Hyp. On the basis of the results from literature (8−10), the z-coordinates are listed (left figure). Right figure shows a schematic description conjectured from WAXS and Raman spectra.

By MPI, the transition metals are distributed inside the collagen with a concentration gradient as a function of the penetration depth, resulting in changing the interhelix bonding state of collagen. Subsequently, the metal infiltrated collagen shows increased strength with increased ductility. A simple explanation cannot be derived from classical composite theory. Experimentally, the mechanical properties of collagen tissues were proven to be primarily dependent on the formation of cross-links between the collagen molecules preventing slippage under load. Charulatha et al. (36) showed that the fracture stress/strain varies in direct/inverse proportion to the cross-link density inside collagen fibrils, respectively. However, Rajini et al. (37) demonstrated the opposite behavior (see Figure S9 in the Supporting Information). In the metal infiltrated collagen, the fracture stress increased in agreement with the results of Chaulatha, and the fracture strain increased in agreement with the results of Rajini, respectively. The mechanical behavior seems to be dependent on the cross-linking agent or the collagen tissues used. From computational results, Buehler (38) reported that higher cross-link density leads to higher yield stress/strain (increased elastic region). If a critical cross-linking density is exceeded, the fracture behavior shifts to molecular fracture resulting from unfolding of collagen molecules caused by rupture of hydrogen bonds. Similar to those results, the metal infiltrated collagen membranes have larger yield stress/strain values, i.e., an increased elastic region as compared to a native collagen membrane (see Figure S10 in the Supporting Information). The metal infiltrated membrane, on the other hand, shows less brittlelike deformation behavior (see Figure S10 and Table S2 in the Supporting Information) than those results. In Buehler's computation, single collagen fibrils with an ideal structure were considered and the deformation behavior was predicted in microscale, whereas in this study, the deformation behaviors of the bulk membranes with entangled collagen fibrils were observed in macroscale. The different scales in observation are believed to cause this difference. Notwithstanding a certain discrepancy between the deformation behavior of metal infiltrated membranes and the above results, it appears reasonable that cross-linking is one of the key factors for the mechanical properties of the collagen membrane. Even though Raman and X-ray scattering results confirmed changes in the molecular structure, we have not yet found ways to clearly show that the metal infiltration increased the cross-linking density. However, considering the increased number of sawtooth peaks (Figure 2) and the increased yield stress/strain value (see Figure S10 and Table S2 in the Supporting Information) of metal infiltrated collagen, from Buehler's results (38) it can be indirectly inferred that the cross-linking density increased after metal infiltration. Chemically, one would also expect an increase, as Hyp with its functional hydroxyl group (−OH) should strongly react with the chemicals used (trimethylaluminum, diethylzinc, and TIP). Furthermore, functional side groups of amino acids X and Z, play a key role for permitting the twisting of the collagen helix. Those groups protrude from the chain and are believed to be exposed to the surrounding and available for intermolecular/interchain interaction, such as cross-links between tropocollagen fibers (39). The collagen of the hen's eggshell membrane contains Gly, Pro and Hyp with 11.1, 11.6, and 1.5% of the total amino acid composition, providing large amounts of functional groups. Additionally, there are further amino acids with functional side groups available for cross-linking (15). The interfibrillar interactions caused by the increased cross-linking density and the intrafibrillar interactions caused by metal-mediated interprotein bonds determines the mechanical deformation behavior of collagen. The deformation behavior of metal infiltrated collagen could possibly be governed by the molecular fracture related to the stretching of the protein backbone and uncoiling of collagen triple helices, which results in increased fracture stress as well as fracture strain, as already suggested by Buehler (39).

CONCLUSION

In summary, metal (Ti, Al,or Zn) infiltration into dried collagen via multiple pulsed vapor phase infiltration (MPI) has induced crystallographic changes of the collagen likely related to interchain hydrogen bonds and has presumably

induced an increase of the interfibrillar cross-linking density. This physical/chemical change by metal infiltration has led to the improved mechanical stability of collagen in a dried state. The process to infiltrate metals into collagen could also be a means to improve the mechanical properties of other collagen-based tissues and scaffolds for medical use (40), although the biocompatibility of such structures and bioactivity still has to be investigated in detail. Furthermore, it remains as a further work to investigate the mechanical behavior of metal infiltrated collagen structures in a wet condition, in order to verify the general practicability of this approach. The infiltrated material in a dried state, however, shows significant improvement of the mechanical properties and might be a step forward in the synthesis and application of biopolymers in every day life, like for robust packaging. The collagen is easily degradable and therefore might be beneficial as replacement for some artificial polymers, helping to preserve a green environment.

Acknowledgment. We dedicate this research article to our former institute director, Prof. Gösele, who passed away in November 2009. This work has received financial support from the German ministry of education and research (BMBF, FKZ 03X5507).

Supporting Information Available: Experimental details, TEM-EDX, Raman, WAXS, SAXS data, and other supporting data (PDF). This material is available free of charge via the Internet at http://pubs.acs.org.

REFERENCES AND NOTES

(1) Cribb, B. W.; Stewart, A.; Huang, H.; Truss, R.; Noller, B.; Rasch, R.; Zalucki, M. P. *Naturwissenschaften* **2007**, *95*, 17–23.
(2) Broomell, C. C.; Zok, F. W.; Waite, J. H. *Acta Biomater.* **2008**, *4*, 2045–2051.
(3) Broomell, C. C.; Mattoni, M. A.; Zok, F. W.; Waite, J. H. *J. Exp. Biol.* **2006**, *209*, 3219–3225.
(4) Lee, S.-M.; Pippel, E.; Gösele, U.; Dresbach, C.; Qin, Y.; Chandran, C. V.; Bräuniger, T.; Hause, G.; Knez, M. *Science* **2009**, *324*, 488–492.
(5) Zhang, L.; Patil, A. J.; Li, L.; Mann, S.; Gösele, U.; Knez, M. *Angew. Chem., Int. Ed.* **2009**, *48*, 4982–4985.
(6) Ricard-Blum, S.; Ruggiero, F.; van der Rest, M. *Top. Curr. Chem.* **2005**, *247*, 35–84.
(7) Ramachandran, G. N.; Kartha, G. *Nature* **1955**, *176*, 593–595.
(8) Rich, A.; Crick, F. H. C. *J. Mol. Biol.* **1961**, *3*, 483–506.
(9) Bella, J.; Eaton, M.; Brodsky, B.; Berman, H. M. *Science* **1994**, *266*, 75–81.
(10) Fraser, R. D. B.; MacRae, T. P.; Suzuki, E. *J. Mol. Biol.* **1979**, *129*, 463–481.
(11) Orgel, J. P. R. O.; Irving, T. C.; Miller, A.; Wess, T. J. *Proc. Natl. Acad. Sci. U. S. A.* **2006**, *103*, 9001–9005.
(12) Gelse, K.; Poschl, E.; Aigner, T. *Adv. Drug Delivery Rev.* **2003**, *55*, 1531–1546.
(13) Wong, M.; Hendrix, M. J.; von der Mark, K.; Little, C.; Stern, R. *Dev. Biol.* **1984**, *104*, 28–36.
(14) Arias, J. L.; Fernandez, M. S.; Dennis, J. E.; Caplan, A. I. *Connect. Tissue Res.* **1991**, *26*, 37–45.
(15) Nakano, T.; Ikawa, N. I.; Ozimek, L. *Poult. Sci.* **2003**, *82*, 510–514.
(16) There are many measurement techniques for the characterization of the mechanical properties of materials such as nanoindentation and AFM. Here, because the sample are not homogenous (collagen inner structure + outer metal oxide films), such techniques were not suitable. Therefore, even though it is a primitive method, the property characterization was performed by means of uniaxial tensile tests.
(17) Rief, M.; Gautel, M.; Oesterhelt, F.; Fernandez, J. M.; Gaub, H. E. *Science* **1997**, *276*, 1109–1112.
(18) Rief, M.; Pascual, J.; Saraste, M.; Gaub, H. E. *J. Mol. Biol.* **1999**, *286*, 553–561.
(19) Smith, B. L.; Schäffer, T. E.; Viani, M.; Thompson, J. B.; Frederick, N. A.; Kindt, J.; Belcher, A.; Stucky, G. D.; Morse, D. E.; Hansma, P. K. *Nature* **1999**, *399*, 761–763.
(20) Oberhauser, A. F.; Marszalek, P. E.; Erickson, H. P.; Fernandez, J. M. *Nature* **1998**, *393*, 181–185.
(21) For the preparation of cross-sectioned sample, we were not able to find out any better method than FIB. Of course, during sectioning, metal (Al, Ti, or Zn) at a certain location might be sputtered out by the ion-beam and re-deposited at the adjacent location. Consequently, this might contribute to the background signal of Ti across the collagen fibril. However, Raman and X-ray analysis clearly confirmed the presence of the metal elements inside the collagen fibrils.
(22) Fernández, A.; Scott, L. R. *Phys. Rev. Lett.* **2003**, *91*, 018102.
(23) Cordier, F.; Grzesiek, S. *J. Mol. Biol.* **2002**, *715*, 739–752.
(24) Spadaro, J. A.; Becker, R. O.; Bachman, C. H. *Nature* **1970**, *225*, 1134–1136.
(25) Martin, J. Y.; Schwartz, Z.; Hummert, T. W.; Schraub, D. M.; Simpson, J.; Lankford, J., Jr.; Dean, D. D.; Cochran, D. L.; Boyan, B. D. *J. Biomed. Mater. Res.* **1995**, *29*, 389–401.
(26) Morra, M.; Cassinelli, C.; Cascardo, G.; Cahalan, P.; Cahalan, L.; Fini, M.; Giardino, R. *Biomaterials* **2003**, *24*, 4639–4654.
(27) Müller, R.; Abke, J.; Schnell, E.; Scharnweber, D.; Kujat, R.; Englert, C.; Taheri, D.; Nerlich, M.; Angele, P. *Biomaterials* **2006**, *27*, 4059–4068.
(28) Rammelt, S.; Illert, T.; Bierbaum, S.; Scharnweber, D.; Zwipp, H.; Schneiders, W. *Biomaterials* **2006**, *27*, 5561–5571.
(29) Yi, F.; Guo, Z.-X.; Zhang, L.-X.; Yu, J.; Li, Q. *Biomaterials* **2004**, *25*, 4591–4599.
(30) Frushour, B. G.; Koenig, J. L. *Biopolymers* **1975**, *14*, 379–391.
(31) Cheng, W.-T.; Liu, M.-T.; Liu, H.-N.; Lin, S.-Y. *Microsc. Res. Tech.* **2005**, *68*, 75–79.
(32) Further literature, which was used for peak assignments, can be found in Table S3 in the Supporting Information.
(33) Beck, K.; Brodsky, B. *J. Struct. Biol.* **1998**, *122*, 17–29.
(34) In the related literature, various reported shifts of the vibrational modes of titanium nitride, in particular in refs 37−42 in the Supporting Information, do not perfectly correspond or even show large differences. In addition, Raman shifts at 578, 488, and 338 cm^{-1} show poor relevance to the shifts of amorphous TiO_2 in the literature.
(35) The location of peaks A, B, and C are close to diffraction peaks of calcite. For the experiments we used collagen membranes extracted from the air-cell region of the hen's egg (see Experimental Section). Decisively, as shown by EDX data in Figure 3B, Ca elements were not detected. Therefore, these peaks presumably do not originate from calcite.
(36) Charulatha, V.; Rajaram, A. *Biomaterials* **2003**, *24*, 759–767.
(37) Rajini, K. H.; Usha, R.; Arumugam, V.; Sanjeevi, R. *J. Mater. Sci.* **2001**, *36*, 5589–5592.
(38) Buehler, M. J. *J. Mater. Res.* **2006**, *21*, 1947–1961.
(39) Buehler, M. J. *Proc. Natl. Acad. Sci. U.S.A.* **2006**, *103*, 12285–12290.
(40) Place, E. S.; Evans, N. D.; Stevens, M. M. *Nat. Mater.* **2009**, *8*, 457–470.

AM100438B